

# 3D PRINTED POROUS CHITOSAN-BASED NANOCOMPOSITE SCAFFOLDS FOR BONE REGENERATION: IN VITRO and IN VIVO STUDY

Doaa H. Abo Dahab<sup>1</sup>\**MSc*, Seham A. Hanafy<sup>2</sup> *PhD*,  
Hanaa M. Aly<sup>3</sup> *PhD*, Hoda M. Eltaher<sup>4</sup> *PhD*, Mohamed M. Abdul-Monem<sup>5</sup> *PhD*

## ABSTRACT

**INTRODUCTION:** Bone regeneration still is a challenging task for the maxillofacial surgeon. Autografts and allografts were two extensively used procedures for bone repair in the past. Tissue engineering is a promising method for employing biomaterials to repair, regenerate, preserve, and enhance the function of injured cells or tissues. Bone scaffold should be designed precisely fitting the 3D shape of the recipient site.

**AIM OF THE STUDY:** The aim of this study was to prepare and characterize chitosan-based hydrogel scaffolds made of chitosan/alginate and chitosan/alginate/nano-hydroxyapatite fabricated by 3D printing and we compared the efficacy of both scaffolds on bone regeneration in a rabbit model.

**MATERIALS & METHODS:** Chitosan-based nanocomposite hydrogel scaffolds were prepared and fabricated by 3D printing. Group I: chitosan/ alginate (control group) and group II: chitosan/ alginate/ nano-hydroxyapatite. Each of the two groups were characterized for in-vitro cytotoxicity, swelling kinetics, hydrolytic degradation, and Fourier Transform Infrared (FTIR). Moreover, the ability of these hydrogel scaffolds to enhance bone regeneration in a rabbit model was performed after 8 weeks using histological analysis.

**RESULTS:** Cell viability results showed no cytotoxicity in either blank (group I) or loaded scaffolds (group II) on fibroblast cells after culture for 24h, 48h & 72h. Group I exhibited higher swelling rate after 5 days. Also, it demonstrated higher degradation rate compared to group II after 28 days. Histological examination of CS/ALG revealed higher bone formation (34%) compared to the HAP loaded scaffolds (26%).

**CONCLUSION:** 3D printed custom-made porous CS/ALG and CS/ALG/HAP scaffolds showed good physical properties and bone regeneration. However, CS/ALG group showed enhanced bone formation compared HAP loaded scaffolds.

**KEYWORDS:** Chitosan, Alginate, Hydroxyapatite, Scaffold, 3D Printing.

**RUNNING TITLE:** 3D Printing Chitosan Nanocomposite Scaffolds for Bone Regeneration.

1 Master of Operative, Faculty of Dentistry, Alexandria University.

2 Professor of Dental Biomaterials, Faculty of Dentistry, Alexandria University.

3 Professor of Oral Biology, Faculty of Dentistry, Alexandria University

4 Associate Professor of Pharmaceutics, Faculty of Pharmacy, Alexandria University.

5 Lecturer of Dental Biomaterials, Faculty of Dentistry, Alexandria University.

\* Corresponding Author:

E-mail: [Dr.do3a2helmy@gmail.com](mailto:Dr.do3a2helmy@gmail.com)

## INTRODUCTION

Trauma and bone illnesses like osteoporosis, arthritis, and cancer can cause maxillofacial bone abnormalities. Bone graft transplantation mostly autografts and allografts. Autografting is frequently associated with a lack of available bone volume for harvesting and donor site morbidity, due to the potential of immune rejection or disease transmission associated with allografting, restoring massive skeletal bone deficiencies is a significant medical challenge (1).

As a result, tissue engineering has shown itself as a feasible option for bone regeneration therapy, particularly in the case of significant bone defects. The 3D matrix used to promote cell adhesion,

proliferation, and differentiation is important for bone tissue regeneration success (1).

Scaffolds serve as templates for tissue regeneration, supporting cells while also transporting waste and growth chemicals. To assure biomimicry, the layouts and properties of human tissues can also be recreated. Biocompatibility, which allows cells to adhere and proliferate, biodegradation profile, mechanical strength, and a network of interconnected pores enabling cell movement, multiplication, and attachment deep within the scaffolds are just a few of the features utilized to determine an ideal scaffold. Such a porous network is necessary for cells in the scaffold's deeper layers to obtain an adequate supply of oxygen and nutrients while simultaneously being capable of rapidly eliminating waste products (2).

Among the biomaterials are natural biomaterials, synthetic polymers and hybrids, ceramics and bioactive glasses used to make tissue-engineered scaffolds. Natural biomaterials have gotten a lot of interest lately due to their low toxicity, absence of a persistent inflammatory response, and propensity to enhance cell viability and differentiation. Chitosan (CS) is a natural polysaccharide made by partially deacetylating chitin, which is found in abundance in crustaceans, shells, insects, and spiders' exoskeletons (3).

The key reasons for chitosan's widespread use as a biomaterial scaffold are its biocompatibility, biodegradability, antibacterial qualities, ability to excite macrophages, stimulate the development of bone, and interact with negatively charged substances as glycosaminoglycans (GAGs) and proteoglycans. (4).

Alginate is an anionic polymer made up of -L-guluronic acid and -D-mannuronic acid sequences identified from brown algal cell walls. Alginate is commonly utilized in bone tissue engineering due to its biocompatibility, hydrophilicity, and biodegradability under normal physiological circumstances. Chitosan and alginate have been combined to make calcium crosslinked hydrogel beads. These beads are formed by the strong ionic interaction between the positively charged amino groups in chitosan and the negatively charged carboxyl groups in alginate (5).

For many years, calcium phosphate ceramics have been routinely employed as bone substitutes. Among these, hydroxyapatite (HAP) has a chemical makeup that is quite similar to that of real bone, and as a result, it has been widely used in bone regeneration research. Calcium phosphate ceramics are known for their high biocompatibility and bioactivity, as they attach to bone and promote tissue growth. Hydroxyapatite is brittle and decomposes slowly (6). Hydroxyapatite nanocrystals bind to bones and boost osteoblast activity, which promotes bone repair (7).

Most common techniques for constructions of scaffolds are gas foaming, solvent-casting particulate-leaching, fibre meshes/fibre bonding, melt moulding, solution casting, emulsion freeze drying, phase separation and freeze drying. These traditional technologies have several drawbacks, including inability to fabricate exact pore size, strong interconnectivity, pore geometry and high mechanical strength (8).

Three-dimensional (3D) printing was developed as a more sophisticated technique to overcome the limitations of these older approaches, and it may result in the fabrication of matrix scaffolds capable of more promoting functional tissue regeneration. Three-dimensional printing has been a viable approach for fabricating scaffolds with great precision and accuracy, to allow the production of biomimetic 3D. 3D printed scaffolds were fabricated by extrusion layer by layer technique (9).

A 3 Dimensional object was printed for the first time by Charles Hull in the year 1983. Hull invented 3D printing which he named "stereolithography". Stereolithography interprets the data in a CAD file by using the file in STL format. Apart from shape the instructions may also include information on color, texture and thickness of the object to be printed. Hull later founded the company 3D Systems which introduced the first commercially available 3D printer named SLA-250 in 1988 (10) then Selective Laser Sintering (SLS), Fused Deposition Modelling (FDM), Digital light processing (DLP), Continuous Liquid Interface Production (CLIP), Multijet printer, Direct Metal Laser Sintering (DMLS), Electron Beam Melting (EBM), Microextrusion Bioprinters (11).

Aim of this study is to determine the ability of chitosan/alginate-based nanocomposite scaffolds loaded with nano-hydroxyapatite to enhance bone regeneration in a rabbit model.

The null hypothesis was that there is no statistically significant difference between the porous 3D printed chitosan/alginate alone scaffolds and chitosan/alginate scaffolds loaded with nano-hydroxyapatite as regard to physical properties and bone regeneration.

## MATERIALS AND METHODS

### 3D printing of chitosan-based scaffolds

Chitosan powder (Acros Organics Co. New Jersey, US); 2.5g (100,000-300,000 mol wt) was mixed with 2.5 g of sodium alginate powder (Sisco Research Laboratories, Mumbai, India) (mol wt 60,000) in 50 ml deionized water by magnetic stirrer (50 round/min) for 10 min. 1000  $\mu$ L of 2% of glacial acetic acid was added and the suspension mix was stirred again using the magnetic stirrer for extra 2 min. The magnetic bar was carefully removed, and the mix was homogenized in ultra-shear homogenizer (1800 round/min) for 15 min to obtain homogenous plain chitosan/alginate (CS/ALG) hydrogel. Different loads of nano hydroxyapatite (Nanostreams Co, Cairo, Egypt; 8nm width 50nm length) in the chitosan / alginate hydrogel were investigated and 200 mg nanohydroxyapatite nanoparticles (HAP NPs) per 4 g hydrogel paste, was the optimal load in terms of the consistency of the formed paste to be employed as the bioink. The composite nanoparticle hydrogel was packed in 5mL sterile disposable plastic Leur lock syringes (11 mm in diameter). The composite hydrogel was 3D printed using a 0.5 mm blunt needle tip linked to a syringe by the custom made Robota 3D printer (ROBOTA equipped with Cura 15.2 software) (Fig.1) by extrusion layer by layer technique at a regulated ambient temperature of 25°C. 3D CAD tool (Tinkercad<sup>®</sup>; Autodesk, California, USA) 3D scaffolds. The printed scaffolds possessed disc shapes of 10 mm diameter and 2 mm height comprising 4 layers each of 0.5

mm height. Printing parameters include 3mm/sec printing speed, 100% fill density and 100% flow capacity of the hydrogel mix from the used syringes. Following printing, crosslinking of the scaffolds was performed via spraying 2 puffs of 5 % v/v glutaraldehyde and 2 % w/v CaCl<sub>2</sub> solution on each surface of the disc scaffolds. The scaffolds were then plotted against dry sterile filter paper to remove the excess glutaraldehyde solution. The preparation was generally conducted under aseptic conditions and the final scaffolds were sterilized for 30 min on each side inside the UV lamp (1 h total), to overcome the penetration limitation of the UV lamp. Scaffolds were then stored in sterile sealed glass containers ready for the tests (12).

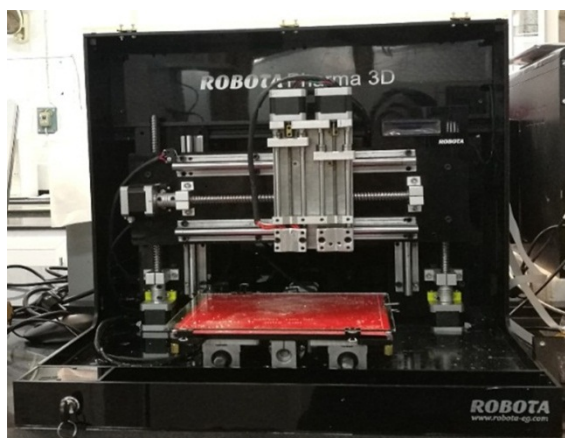


**Figure 1:** Custom-made 3D printer ROBOTA equipped with Cura 15.2 software, Alexandria, Egypt.

## Laboratory characterization of hydrogel scaffolds

### A. Cytotoxicity

#### A.1. Isolation and Culture of Gingival tissue

A sample of keratinized gingival tissue was taken from donors undergoing crown lengthening procedure under local anesthesia. Donors provided signed informed consent in accordance with a protocol approved by the Ethical Committee of the Faculty of Dentistry at Alexandria University in Egypt. Gingival samples are placed in 50 ml sterile falcon tube filled with phosphate buffered saline (PBS) (Biowest, Business Park Lane, USA) + 3% penicillin/streptomycin/amphotericin (containing 10,000 µg/mL streptomycin; 10,000 IU/mL penicillin and 25 µg/mL amphotericin B, Lonza) to the Center of Excellence for Research in Regenerative Medicine and its Applications (CERRMA in Faculty of Medicine in Alexandria University).

Under sterile conditions in a safety cabinet Class II, the tissue sample was de-epithelialized and divided into small fragments 1x1 mm. Tissue fragments were cultured in tissue culture dishes in low glucose Dulbecco's modified Eagle's medium (LG-DMEM) supplemented with, 2 mm L-glutamine, 10% fetal bovine serum and 1% penicillin/streptomycin

(Biowest, Business Park Lane, USA) and left at 37 °C with 5% CO<sub>2</sub> in humidified incubator.

Every 2-3 days, the growth media were replaced. Growth of the tissue explanted fibroblasts reached 80%–85% confluence after an average of 14 days. The cells were detached from the monolayer using trypsin EDTA. (1 mM EDTA, 0.25% trypsin) (Biowest, Business Park Lane, USA) and sub-cultured in tissue flasks in same conditions till reached passage 4 then used for running the experiment's tests (13).

#### A.2. MTT assay

Cell viability was determined using MTT (3-(4,5-dimethylthiazol-2-yl)-2,5-diphenyl-2H-tetrazolium bromide) assay. Human gingival fibroblast cells at passage 5 were planted at density  $5 \times 10^3$  cells per well in 96-well plates, kept in 100 µL of complete culture medium (CCM) for each well following a 24-hour incubation period, cells were incubated for a further 24 hours, 48 hours, and 72 hours with a 48-hour 1 with 48-hour conditioned media, media that had been pre-incubated with various hydrogel and nanocomposite hydrogel scaffolds, or plain CCM for the control group. After removing the medium, cells were incubated with 100 L MTT solution (0.5 mg/ml in CCM) at 5% CO<sub>2</sub> and 37°C for 4 hours. Finally, MTT solution was thrown away and the formazan crystals were dissolved in 100 l dimethyl sulfoxide (DMSO) and then agitated for 15 minutes. The absorbance at a wavelength of 570 nm was determined using a microplate reader (ELX 800; Biotek, California, USA). After normalising the optical density (OD) values for all groups to the OD value for the control group, the percentage cell viability statistics were obtained (13).

#### B. Swelling Kinetics

Hydrogel and nanocomposite hydrogel scaffolds were prepared to measure swelling kinetics based on the equilibrium swelling theory state of hydrogels. The scaffolds were immersed in distilled water and weighed using a sensitive balance at intervals while the weight and volume of the scaffolds increased owing to swelling. This method was repeated until no change in weight was seen (14).

The swelling % was given as follows:

$$\text{Swelling (\%)} = (W_s - W_0 / W_0) \times 100$$

Where, W<sub>s</sub> is the weight of swollen scaffold and W<sub>0</sub> is the weight of dried scaffold.

#### C. Hydrolytic Degradation

Hydrogel and nanocomposite hydrogel scaffolds were used to measure the degradation percentage. At 37°C and a pH of 7.4, scaffolds were placed in phosphate buffer solution (PBS). Every three days, the medium was replaced. After 28 days, samples were obtained and weighed. (15).

The degradation percentage (%W<sub>L</sub>) was determined using the following equation:

$$\%W_L = ((W_i - W_f) / W_i) \times 100\%$$

Where,  $W_i$  is the scaffold's initial dry weight and  $W_f$  is the dried scaffold's weight following incubation in phosphate buffer solution.

#### D. Fourier Transform Infrared (FTIR)

To explore the creation of crosslinked networks from glutaraldehyde and calcium chloride blends, FTIR (Bruker Tensor 37, Germany) was used to analyse functional groups in hydrogels and nanocomposite hydrogels. With a resolution of  $2\text{ cm}^{-1}$ , spectra were acquired over  $4000\text{--}650\text{ cm}^{-1}$ . (13).

#### In-vivo calvarial bone defect experimental study

After getting approval from the Ethical Committee [IRB NO 00010 556-IORG 0008839] in Faculty of Dentistry in Alexandria University in Egypt, in vivo experiment was conducted.

In vivo experiments were conducted at the Poultry Research Center, Faculty of Agriculture, Alexandria University, Egypt. eighteen New Zealand white rabbits were used in this study, divided into two groups. The rabbits taken were six months old, male, weighed around three kilograms, and had good systemic health. They were housed in bracket cages at a temperature of  $25^\circ\text{C}$  for one week before the operation at the animal house on a soft diet and vitamins for adaption.

All surgical procedures were performed in an aseptic environment and under general anesthesia. Intramuscular injections of ketamine in conjunction with xylazine at doses of  $35\text{ mg/kg}$  and  $5\text{ mg/kg}$  of body weight were used to anaesthetize rabbits. Prior to surgery, the skin was exposed and it was covered with antiseptic iodine-based solution. A skin incision was created above the cranial vault. (Fig.2 A) and cutaneous flap was elevated (Fig.2 B) (16). To remove bone debris, the bone cavity was cleansed with saline and dried with gauze. The bone defects were filled with sterile freeze dried hydrogel and the nanocomposite hydrogel scaffolds of each of the two groups (Fig.2 E). The periosteum was realigned, and the skin was sutured (Fig.2 F) (17). To avoid infection and relieve pain,  $5\text{ mg/kg}$  broad-spectrum antibiotic intramuscularly postoperatively and analgesic  $0.1\text{ mg/kg}$  were given daily for 10 days. The weight gain and cage behavior of the rabbits were monitored daily. The wounds were allowed to heal naturally for 8 weeks before being euthanized with an overdose of diethyl ether and having the skull chopped to certify death. Undecalcified sections were prepared by fixation in 10% phosphate buffered formalin solution for 24 hours then followed by dehydration in increasing concentrations of ethyl alcohol (70-80-90-100%), 24 hours in each concentration, and then for 24 hours, clear in xylene. Following that, the specimens were immersed in methyl methacrylate (MMA) for three days. For the next three days, MMA with  $0.1\text{ mg}$  benzoyl peroxide (BP) /  $10\text{ mL}$  was used. Finally, specimens were imbedded in MMA with  $0.25\text{ mg}$  BP per  $10\text{ mL}$  and allowed to polymerize slowly for 7 days in a water bath at  $32^\circ\text{C}$ . Using a microtome precision cutter,  $100\text{ m}$  thick section was cut from each specimen, which were subsequently polished with silicon carbide paper. Finally, For 3 minutes each, slices were dyed with methylene blue and acid fuchsin (18). The histology of newly regenerated bone in the defect

area was studied using a light microscope on undecalcified sections.

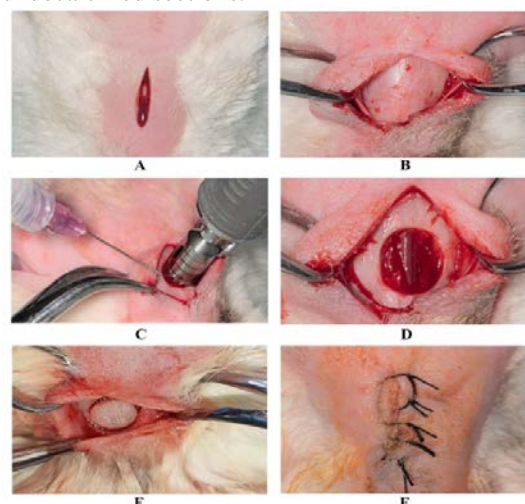


**Figure 2:** Surgical procedure in the cranial vault and placement of the 3D printed scaffold.

A) Incision in the skin. B) Cutaneous flap raised and reflected. C) Creation of a circular bone defect,  $10\text{ mm}$  in diameter, with a trephine bur using a low-speed hand piece under sterile saline irrigation. D) Circular Bone defect,  $10\text{ mm}$  in diameter. E) The bone defect was filled with the nano composite hydrogel scaffolds. F) Skin was sutured.

To perform histomorphometric analysis, photomicrographs of the undecalcified sections at  $40\times$  magnifications were taken with a digital camera attached to a light microscope. The area of new bone trabeculae generated in a location of interest was calculated using Image J software (ROI area). New bone area % was calculated according to the following equation (19).

New bone area % = New trabeculae area / ROI area

#### Statistical analysis

SPSS software package version 20.0 was used to collect and analyses data. The two groups were compared using one-way analysis of variance (ANOVA) with the F-test, and pairwise comparisons were made using Tukey's (Post Hoc) test. Statistical significance was defined as a P value of less than 0.05.

## RESULTS

### In-vitro characterization

Cell viability results indicated no fibroblast cytotoxicity for loaded or unloaded hydrogels after culture for 24h, 48h & 72h. After 24h group I (CS/ALG) had higher percentage of cell proliferation compared to group II (CS/ALG/HAP) but with non-significant statistical difference. However, after 48h and 72h, the unloaded control group I demonstrated statistically significant higher cell proliferation percentage compared to the hydroxyapatite loaded group (Table 1 & Fig.3 A). The equilibrium swelling state for the two groups was reached after 5 days regardless of their composition. Group I showed higher swelling rate

than group II. The results were statistically significant (Table 1 & Fig.3 B). Group I showed higher degradation rate than group II after 28 days. The results were statistically significant (Table 1 & Fig.3 C). FTIR spectra of chitosan showed NH at wavelength 658 cm<sup>-1</sup>, C–O–C at wavelength 1156 cm<sup>-1</sup>, CH<sub>2</sub> at wavelength 2880 cm<sup>-1</sup>, OH at wavelength 3281 cm<sup>-1</sup> and C=O was observed at 1656, 1596, and 1424 cm<sup>-1</sup> (Fig. 4 A). On the other hand, FTIR spectra of alginate showed mannuronic acid at wavelength 893 cm<sup>-1</sup> and the uronic acid at wavelength 944 cm<sup>-1</sup>, OH group at wavelength 2930-3402 cm<sup>-1</sup> and CH<sub>2</sub> at wavelength 2154 cm<sup>-1</sup> (Fig. 4 B). For nano hydroxyapatite, peaks characteristic of (PO<sub>4</sub>)<sub>3</sub> group were shown at 567 and 603 cm<sup>-1</sup> and (CO<sub>3</sub>)<sub>2</sub> intensive peaks between 1420 and 1455 cm<sup>-1</sup> (Fig. 4 C). FTIR spectrum of chitosan/alginate scaffold showed OH stretching at 3621 cm<sup>-1</sup>. NH bending occurred at 1598 cm<sup>-1</sup>. These changes confirm the formation of chitosan/alginate gel as a result of the interaction between the negatively charged alginate carbonyl group and positively charged chitosan amino group (Fig.4 D). Composite chitosan/alginate/hydroxyapatite scaffold showed amide at 1600 cm<sup>-1</sup> and phosphate stretching at 1038 cm<sup>-1</sup>. This was similar to HAP powder sample with hydroxyl vibrations occurred at 1600 cm<sup>-1</sup>. (Fig. 4 E).

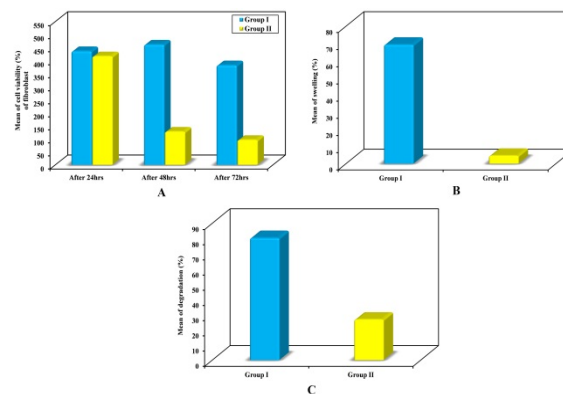


**Figure 3:** Comparison between CS/ALG (Group I) and CS/ALG/HAP (Group II) according to A. % Cell Viability relevant to untreated control B. Swelling (%) after 5 days, C. Degradation (%) after 28 days. Data are represented as average ± SD.

**Table (1):** Comparison between the two studied groups according to cell viability (%) of fibroblast, Swelling (%), Degradation (%) and Bone Formation

Cell viability (%) of fibroblast	Group I (n = 9)	Group II (n = 9)	P
<b>After 24 hrs.</b>			
Mean ± SD.	436.4 ± 76.3	416.5 ± 18.5	0.466
Median (Min. – Max.)	372.1 (372.1 – 516.9)	400.9 (400.9 – 436)	
<b>After 48 hrs.</b>			
Mean ± SD.	461.6 ± 5.9	127.3 ± 6.5	<0.001*
Median (Min. – Max.)	466.6 (455.5 – 466.6)	121.8 (121.8 – 134.2)	
<b>After 72 hrs.</b>			
Mean ± SD.	382.2 ± 143.1	95.5 ± 1.3	<0.001*
Median (Min. – Max.)	261.5 (261.5 – 533)	94.4 (94.4 – 96.8)	
<b>Swelling (%)</b>			
Mean ± SD.	69.3 ± 18.3	4.6 ± 1.3	<0.001*
Median (Min. – Max.)	70 (47.8 – 90)	5.2 (2.9 – 5.7)	
<b>Degradation (%)</b>			
Mean ± SD.	80.4 ± 1.5	26.7 ± 8.5	<0.001*
Median (Min. – Max.)	79.7 (78.6 – 82.3)	24.1 (18.4 – 37.5)	
<b>Bone Formation (%)</b>			
Mean ± SD.	29.9 ± 4.6	21.5 ± 3.6	0.001*
Median (Min. – Max.)	31.2 (25.5 – 37.9)	22 (15.7 – 25.5)	

SD: Standard deviation

t: Student t-test

p: p value for comparing between the studied groups

\*: Statistically significant at p ≤ 0.05

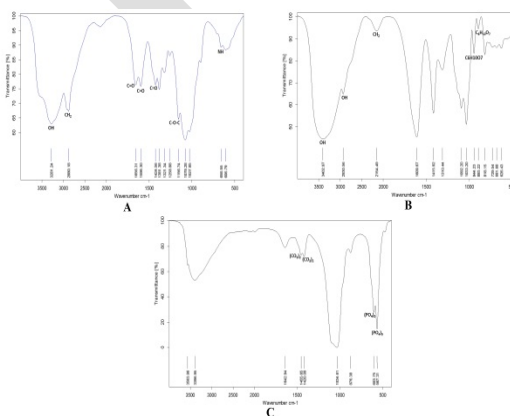


**Figure 4:** Fourier Transform Infrared Spectroscopy (FTIR) spectra of A) Chitosan. B) Alginate. C) Hydroxyapatite D) CS/ALG scaffold E) CS/ALG/HAP scaffold.

**In-vivo calvarial bone defect**

Histological examination of the undecalcified sections of all groups, showed bone formation in both groups but with different amounts. Bone formation in groups I and group II occurred in the form of islands. The amount of bone formation in group I was greater than group II as the scaffold in group I degraded faster than group II (Fig. 5). Statistical analysis of histomorphometric results revealed statistically significant difference between the two groups. Group I (CS/ALG) showed higher bone formation; 34%, while group II (CS/ALG/HAP) showed the less bone forming ability; 26% new bone (Table 1 & Fig.6).

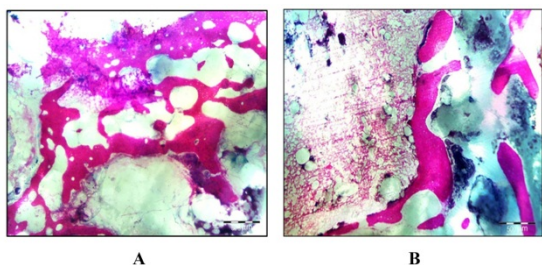


**Figure 5:** Photomicrographs of the defect areas showing the various amounts of new bone formation at the end of 8 weeks after implantation with methylene blue & acid fuchsin stain at magnification  $\times 40$ , Scale bars 500  $\mu\text{m}$ . A) Group I (CS / ALG). B) Group II (CS / ALG / HAP). Bone formation (black arrow), scaffold (blue arrow).

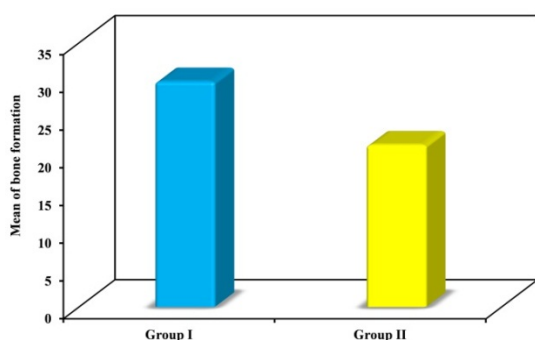


**Figure 6:** Comparison between the two studied groups according to bone formation.

## DISCUSSION

In this study 3D printed custom-made porous chitosan/alginate hydrogel scaffolds loaded with nano-hydroxyapatite showed good physical properties and bone regeneration.

Cell viability results indicated no cytotoxicity for hydrogels used in this study on fibroblast after culture. These results were in agreement with the results obtained by Venkatesan et al, (2014) as they proved that chitosan/alginate scaffolds were biocompatible and non-cytotoxic in nature (20). As well as Wong *et al*, (2020) found that chitosan/alginate scaffolds gave promising cell viability percentage (21). Also, this study results agreed with Kumar *et al*, (2020) who proved that chitosan/nano-hydroxyapatite scaffolds had good compatibility with fibroblast cells which were able to adhere, proliferate, and migrate through the porous structure (22).

The results of the equilibrium swelling of the two hydrogels was reached after 5 days and they revealed that group I (CS/ALG) showed the higher swelling rate compared to the HAP-loaded group. These results agreed with Bibi *et al*, (2019) who stated that the films of (CS/ALG) have high swelling ability due to greater free hydrophilic groups. This highest value and maximal swelling capacity of (CS/ALG) related to the presence of the

most hydrophilic functional groups in the polymer blend (23).

The present study showed that the results of swelling kinetics and degradation rate decreased with the addition of HAP. These results agreed with Liu et al, (2021) who stated that when HAP gradually increase, the gravity factor is more important than the hydrophilic factor for the scaffold's water absorption and swelling ability in which a gradual decrease of the water absorption, swelling ability and degradation rate is observed (24).

Concerning FTIR spectrum of the scaffolds used in this study their results agreed with previous reports. FTIR spectrum of chitosan showed characteristic peaks at 658  $\text{cm}^{-1}$  which represents NH, 1156  $\text{cm}^{-1}$  which represents C–O–C, 2880  $\text{cm}^{-1}$  which represents  $\text{CH}_2$ , 3281  $\text{cm}^{-1}$  which represents OH and 1656  $\text{cm}^{-1}$ , 1596  $\text{cm}^{-1}$ , 1424  $\text{cm}^{-1}$  which represents C=O these results agreed with Varma et al, (2020) (25), FTIR spectrum of alginate showed characteristic peaks at 893  $\text{cm}^{-1}$  which represents mannuronic acid, at 944  $\text{cm}^{-1}$  which represents uronic acid, at 2930-3402  $\text{cm}^{-1}$  which represents OH group and at 2154  $\text{cm}^{-1}$  which represents  $\text{CH}_2$  these results agreed with Aprilliza M (2017) (26). For FTIR spectrum of HAP NPs showed characteristic peaks at 567 and 603  $\text{cm}^{-1}$  which represents  $(\text{PO}_4)_3$  group and at intensive peaks between 1420 and 1455  $\text{cm}^{-1}$  which represents  $(\text{CO}_3)_2$  these results agreed with Gheisari H *et al*, (2015) (27), FTIR spectrum of chitosan/alginate scaffold showed characteristic peaks at 3621  $\text{cm}^{-1}$  which represents OH and 1598  $\text{cm}^{-1}$  which represents NH these results agreed with Baysal *et al*, (2013) (28), as well as FTIR spectrum of chitosan/alginate/hydroxyapatite scaffold showed characteristic peaks at 1600  $\text{cm}^{-1}$  which represents amide, 1038  $\text{cm}^{-1}$  which represents phosphate. For HAP powder sample, 1600  $\text{cm}^{-1}$  which represents hydroxyl vibrations these results agreed with Han J et al. (2010) (29).

The histological findings of this study at the end of the 8<sup>th</sup> week showed surgical defect areas in the two examined groups with various amount of new bone formed. The amount of formed bone was greater in group I scaffolds than hydroxyapatite-loaded scaffolds-group II and this was confirmed by the histomorphometric analysis of this study which revealed statistically significant difference between the two groups. The high bone forming ability of group I (CS/ALG) shown in this study agreed with RajendiranRajesh *et al*. (2017) who proved that alginate is important for the production of 3D scaffold materials in bone tissue engineering because it mimics the natural extracellular matrix, and that bone forming osteoblast cells rapidly adhered to the chitosan-alginate scaffold and proliferated well (30). It also enhances osteogenic development and mineralization, as well as preventing inflammatory responses (31).

The present study agreed with Sukpaita et al, (2021) who stated that chitosan is used as a 3D scaffold in bone tissue creation because it stimulates osteogenic differentiation and mineralization while also preventing inflammation (31). In accordance to Chatzipetros et al, (2018) who proved that nano-Hydroxyapatite/Chitosan scaffolds on guided bone regeneration in rat calvarial critical-sized defects are promising, as the scaffold promotes cell proliferation, growth and migration (32).

Regarding group II; CS/ALG/HAP, they showed less bone regeneration than group I. This result was consistent with Rojbani *et al*, (2011) as they confirmed that  $\alpha$ -TCP,  $\beta$ -TCP, and HAP are osteoconductive materials which act as space maintainer for the bone development when applied to a rat calvarial lesion.  $\alpha$ -TCP offers the advantage of a faster rate of degradation, which allows for greater bone growth followed by  $\beta$ -TCP then HAP which have the least degradation rate and so the least new bone formation (33).

Chitosan-, alginate-, and gelatin-based composites revealed promising results for BTE applications. The addition of other synthetic or natural polymers, ceramics, antibacterial substances, or growth factors enhanced the cell behavior (attachment, proliferation, and differentiation), which led to promising in vitro and in vivo results. Moreover, they improved the mechanical properties and the degradation rate, which are fundamental for BTE applications. To assure the success of BTE composites, in vivo tests should be carried out more frequently. Moreover, more animal models should be taken into consideration for in vivo tests, to assure relevant results for future research. Furthermore, preclinical, and clinical tests are required to facilitate the entrance of BTE biomaterials in the biomedical area. If promising BTE biomaterials would be approved as treatment methods, the evolution of biomedical field would be enormous (34).

3D printing has achieved many tissue engineering requirements that are needed for developing bio fabrication systems. There are various strategies of the 3D printing technique in developing scaffolds for tissue regeneration that could be promising for clinical use in the future. the scaffold preparation by electrospinning technique could be a promising approach in tissue regeneration. The fabricated cell-laden scaffolds subjected to photopolymerization revealed that the UV radiated 3D printed scaffolds have shown increased cell viability compared to bare scaffolds. The scaffolds prepared by both inkjet and extrusion-based 3D printing techniques showed significant impact on cell adherence, proliferation, and differentiation of new bone tissues evident by in vitro and in vivo studies. The 3D printed samples with growth factors have resulted in enhanced ECM, collagen content, and

high GAG content for cell growth and new tissue formation. Due to some drawbacks in the preparation of 3D scaffolds for tissue regeneration, laser printing 3D technique, inkjet, and extrusion-based 3D printing were widely used (35).

## CONCLUSIONS

All materials used in the study were promising biomaterials which enhance bone regeneration. However, the amount of the bone in group I was greater than group II this is due to slow degradation rate of HAP.

## CONFLICT OF INTEREST

The authors declare that they have no financial or personal conflicts of interest.

## FUNDING STATEMENT

The authors received no specific funding for this work.

## REFERENCES

1. O'brien FJ. Biomaterials & scaffolds for tissue engineering. *Mater Today*. 2011;14:88-95.
2. Ikada Y. *Tissue engineering: fundamentals and applications*. United States: Elsevier; 2011.
3. Jayakumar R, Prabakaran M, Nair S, Tokura S, Tamura H, Selvamurugan N. Novel carboxymethyl derivatives of chitin and chitosan materials and their biomedical applications. *Prog Mater Sci*. 2010;55:675-709.
4. Huang Y, Onyeri S, Siewe M, Moshfeghian A, Madihally SV. In vitro characterization of chitosan-gelatin scaffolds for tissue engineering. *Biomaterials*. 2005;26:7616-27.
5. Chen L, Tian Z, Du Y. Synthesis and pH sensitivity of carboxymethyl chitosan-based polyampholyte hydrogels for protein carrier matrices. *Biomaterials*. 2004;25:3725-32.
6. Lv Q, Nair L, Laurencin CT. Fabrication, characterization, and in vitro evaluation of poly(lactic acid glycolic acid)/nano-hydroxyapatite composite microsphere-based scaffolds for bone tissue engineering in rotating bioreactors. *J Biomed Mater Res A*. 2009;91:679-91.
7. Noor Z. Nanohydroxyapatite application to osteoporosis management. *J Osteoporos*. 2013;2013:679025.
8. Wüst S, Müller R, Hofmann S. Controlled Positioning of Cells in Biomaterials-Approaches Towards 3D Tissue Printing. *J Funct Biomater*. 2011;2:119-54.
9. Peltola SM, Melchels FP, Grijpma DW, Kellomäki M. A review of rapid prototyping techniques for tissue engineering purposes. *Ann Med*. 2008;40:268-80.
10. Ventola CL. Medical Applications for 3D Printing: Current and Projected Uses. *P T*. 2014;39:704-11.

11. Kohli Tarika M. 3D printing in dentistry—An overview. *Acta Sci Dent Sci.* 2019;3:35-41.
12. El-Habashy SE, El-Kamel AH, Essawy MM, Abdelfattah EZA, Eltaher HM. Engineering 3D-printed core-shell hydrogel scaffolds reinforced with hybrid hydroxyapatite/polycaprolactone nanoparticles for in vivo bone regeneration. *Biomater Sci.* 2021;9:4019-39.
13. El-Habashy SE, Eltaher HM, Gaballah A, Zaki EI, Mehanna RA, El-Kamel AH, et al. Hybrid bioactive hydroxyapatite/polycaprolactone nanoparticles for enhanced osteogenesis. *Mater Sci Eng C.* 2020;119:111599.
14. Akakuru O, Isiuku B. Chitosan hydrogels and their glutaraldehyde-crosslinked counterparts as potential drug release and tissue engineering systems-synthesis, characterization, swelling kinetics and mechanism. *J Phys Chem A.* 2017;7:1-7.
15. Georgopoulou A, Papadogiannis F, Batsali A, Marakis J, Alpantaki K, Eliopoulos AG, et al. Chitosan/gelatin scaffolds support bone regeneration. *J Mater Sci Mater Med.* 2018;29:59.
16. Nagata MJ, Melo LG, Messoria MR, Bomfim SR, Fucini SE, Garcia VG, et al. Effect of platelet-rich plasma on bone healing of autogenous bone grafts in critical-size defects. *J Clin Periodontol.* 2009;36:775-83.
17. Nuntanaranont T, Bounmanatham B, Kamolmatyakul S. Effect of chitosan scaffold on bone healing in rabbit calvarial defect. *Songklanakarin J Sci Technol.* 2018;40: 792-7.
18. Goldschlager T, Abdulkader A, Kerr J, Boundy I, Jenkin G. Undecalcified bone preparation for histology, histomorphometry and fluorochrome analysis. *J Vis Exp.* 2010;35:1707.
19. Egan KP, Brennan TA, Pignolo RJ. Bone histomorphometry using free and commonly available software. *Histopathology.* 2012;61:1168-73.
20. Venkatesan J, Bhatnagar I, Kim SK. Chitosan-alginate biocomposite containing fucoidan for bone tissue engineering. *Mar Drugs.* 2014;12:300-16.
21. Wong SHM, Lim SS, Tiong TJ, Show PL, Zaid HFM, Loh HS. Preliminary In Vitro Evaluation of Chitosan-Graphene Oxide Scaffolds on Osteoblastic Adhesion, Proliferation, and Early Differentiation. *Int J Mol Sci.* 2020;21:5202.
22. Kumar P, Saini M, Dehiya BS, Umar A, Sindhu A, Mohammed H, et al. Fabrication and in-vitro biocompatibility of freeze-dried CTS-nHA and CTS-nBG scaffolds for bone regeneration applications. *Int J Biol Macromol.* 2020;149:1-10.
23. Bibi A, Rehman SU, Faiz R, Akhtar T, Nawaz M, Bibi S. Effect of surfactants on swelling capacity and kinetics of alginate-chitosan/CNTs hydrogel. *Mater Res Express.* 2019;6:085065.
24. Liu D, Liu Z, Zou J, Li L, Sui X, Wang B, et al. Synthesis and Characterization of a Hydroxyapatite-Sodium Alginate-Chitosan Scaffold for Bone Regeneration. *Front Mater.* 2021;8:648980.
25. Varma R, Vasudevan S. Extraction, Characterization, and Antimicrobial Activity of Chitosan from Horse Mussel *Modiolus modiolus*. *ACS Omega.* 2020;5:20224-30.
26. Helmiyati H, Aprilliza M. Characterization and properties of sodium alginate from brown algae used as an ecofriendly superabsorbent. *IOP Conf Ser Mater Sci Eng.* 2017;188:012019
27. Gheisari H, Karamian E, Abdellahi M. A novel hydroxyapatite-Hardystonite nanocomposite ceramic. *Ceram Int.* 2015;41:5967-75.
28. Baysal K, Aroguz AZ, Adiguzel Z, Baysal BM. Chitosan/alginate crosslinked hydrogels: preparation, characterization and application for cell growth purposes. *Int J Biol Macromol.* 2013;59:342-8.
29. Han J, Zhou Z, Yin R, Yang D, Nie J. Alginate-chitosan/hydroxyapatite polyelectrolyte complex porous scaffolds: preparation and characterization. *Int J Biol Macromol* 2010;46:199-205.
30. Rajesh R, Ravichandran YD, Kuo YC. Alginate in Bone Tissue Engineering. In: Venkatesan J, Anil S, Kim SK (eds). *Seaweed Polysaccharides Isolation, Biological and Biomedical Applications.* United States: Elsevier; 2017. 349-68.
31. Sukpaita T, Chirachanchai S, Pimkhaokham A, Ampornaramveth RS. Chitosan-Based Scaffold for Mineralized Tissues Regeneration. *Mar Drugs.* 2021;19:551.
32. Chatzipetros E, Christopoulos P, Donta C, Tosios KI, Tsiambas E, Tsiourvas D, et al. Application of nano-hydroxyapatite/chitosan scaffolds on rat calvarial critical-sized defects: A pilot study. *Med Oral Patol Oral Cir Bucal.* 2018;23:e625-32.
33. Rojbani H, Nyan M, Ohya K, Kasugai S. Evaluation of the osteoconductivity of  $\alpha$ -tricalcium phosphate,  $\beta$ -tricalcium phosphate, and hydroxyapatite combined with or without simvastatin in rat calvarial defect. *J Biomed Mater Res A.* 2011;98:488-98.
34. Zarif ME. A review of chitosan-, alginate-, and gelatin-based biocomposites for bone tissue engineering. *Biomater. Tissue Eng Bull.* 2018;5:97-109.
35. Sun F, Sun X, Wang H, Li C, Zhao Y, Tian J, et al. Application of 3D-Printed, PLGA-Based Scaffolds in Bone Tissue Engineering. *Int J Mol Sci.* 2022;23:5831.